Wear xxx (xxxx) xxx

Contents lists available at ScienceDirect

Wear

journal homepage: www.elsevier.com/locate/wear

Recreating cobalt – based glaze layers through thermal spraying for extreme environments

Andre R. Mayer [a,*], Omar Zouina [b], Martin Dienwiebel [b,c], Christian Moreau [a], Pantcho P. Stoyanov [d,**]

[a] Department of Mechanical, Industrial & Aerospace Engineering, Concordia University, Montreal, Quebec, Canada
[b] Karlsruhe Institute of Technology KIT, Institute for Applied Materials, MicroTribology Center μTC, Strasse Am Forum 5, 76131 Karlsruhe, Germany
[c] Fraunhofer-Institute for Mechanics of Materials IWM, MicroTribology Center μTC, Woehlerstrasse 11, 79108 Freiburg, Germany
[d] Department of Chemical and Materials Engineering, Concordia University, Montreal, Quebec, Canada

ARTICLE INFO

Keywords:
Extreme tribology
Glaze layer
Wear
Suspension plasma spray
Superalloys
Oxide-based coatings
Gas turbine engines

ABSTRACT

The demanding environments often encountered in engineering applications require the development of advanced materials capable of resisting to extreme conditions. Gas turbine engines is one example of application where tribological interfaces are exposed to extreme fluctuations in temperatures and harsh contact conditions. To overcome these challenges, materials and coatings are developed with specific characteristics tailored for the application. Certain materials attract special attention due to their capacity for developing specific tribolayers (i.e., glaze layers) during service at high temperatures, reducing their wear. For instance, cobalt-chromium alloys are strategically employed in gas turbine engines when temperature and wear are concerns due to their capacity for forming such lubricious glaze layers. Despite the protective effect of these glazes, their formation mechanism still relies on previous surface wear, making the break-in period of components challenging. More recently, the development of coatings based on the chemistry of these glazes has generated significant interest with the main purpose to be applied to protect other surfaces (e.g., nickel-based alloys) or to reduce the break-in period of cobalt-chromium alloys. Therefore, this study focuses on the development and analysis of a cobalt oxide thermally sprayed coating and its comparison to Haynes 25 and Inconel 718. Ball-on-flat at 600 °C and 800 °C tests were performed to evaluate the coatings' suitability for extreme environments. The results have shown a better performance of the cobalt oxide coating at lower temperatures and comparable performance to Haynes 25 at higher temperatures, where a glaze was formed over Haynes 25. More detailed analysis of the glaze layer formed on Haynes 25 revealed a mixed glaze formed with the debris originating from the Haynes 25 and the counterface (Inconel 718).

1. Introduction

Gas turbine engines are a critical component in the aerospace industry, where materials must exhibit exceptional wear resistance, especially at elevated temperatures. Higher operating temperatures are anticipated due to improvements in engine efficiency [1], driven by economic factors such as reduced fuel consumption and costs [2], as well as environmental goals like lowering emissions [3]. The push for higher operating temperatures introduces complex engineering challenges, as multiple tribological interfaces (i.e., where moving parts interact) are subject to significant wear [4]. As a result, there is a need for the development of new surfaces and materials that can resist these demanding conditions, as the integrity and longevity of engine components are directly impacted by their ability to resist wear and tear under such extreme environments.

High temperatures were among the first challenges to be addressed during the development of early gas turbine engines. In 1929, Bedford, Pilling, and Merica significantly improved creep resistance by adding small amounts of titanium and aluminum to an 80Ni-20Cr alloy [5]. Since then, various nickel-based superalloys have been developed [6].

This article is part of a special issue entitled: WOM2025 published in Wear.

* Corresponding author.
** Corresponding author.
E-mail addresses: andre.mayer@mail.concordia.ca (A.R. Mayer), pantcho.stoyanov@concordia.ca (P.P. Stoyanov).

https://doi.org/10.1016/j.wear.2025.205972
Received 16 September 2024; Received in revised form 6 February 2025; Accepted 8 February 2025
Available online 25 February 2025

Table 1
Spraying parameters of the CoO thermally sprayed coating.

Coating	Spraying Distance (mm)	Feed Rate (ml/min)	Current (A)	Passes	Ar, N_2, H_2 (%)	Total Gas Flow (lpm)	Power (kW)
CoO	75	45	170	30	80, 10, 10	220	63

These alloys are highly valued for their ability to maintain mechanical properties at elevated temperatures [7], making them a common choice when high-temperature mechanical resistance is required. Another material option for gas turbine engines are the cobalt-based alloys, which generally exhibit excellent wear resistance at high temperatures [8]. These alloys are particularly attractive because they form a glaze layer when subjected to high-temperature wear, which significantly reduces wear [9]. This glaze forms through debris sintering and develops a layered structure of cobalt- and chromium-based oxides, with its top surface (i.e., the surface exposed to wear) composed mostly of cobalt oxide [10]. However, the use of cobalt-based alloys is still limited due to several factors, including higher cost and density [11], frequent supply shortages [12], and increasing demand [13]. As a result, nickel-based alloys continue to be widely used in the aero-engine sector [14].

To address the limitations typically associated with metallic alloys (e.g., oxidation at high temperatures) and improve wear resistance, various surface enhancement techniques can be applied. A common approach in the aerospace sector is the use of thermally sprayed coatings [15], which allows coating the surface with materials tailored for the application. Coatings for clearance control [16], thermal barrier [1], and prevention of fretting wear [17] are among the possible applications of thermally sprayed coatings for gas turbine engines. Previous studies have shown that cobalt oxide coatings, one of the major components in the glaze layers formed on Haynes 25 [10], can be applied by thermal spray techniques and promising wear characteristics were observed. Roy et al. has observed that CoO coatings presented better wear resistance compared to NiO in terms of wear [18], and when comparing it to other oxides, it was also observed a better performance in terms of wear [19]. Another study, where CoO, Cr_2O_3, and a mixed composition were sprayed, showed that the solely sprayed CoO coating presented the best overall wear performance [20]. It was observed wear of the CoO coating at room temperature, and at high temperature wear significantly decreased. In this study the wear was observed mostly on the counterfaces, with the CoO having the lowest counterface wear, making it particularly suitable for applications where the opposite surface is sensitive to wear. Nonetheless, the comparison of such coatings with commonly used alloys in the manufacturing of gas turbine components (e.g., cobalt- and nickel-based superalloys) has not yet been explored. In general, the CoO coatings have shown promising wear resistance when compared to other oxide-based coatings, whether sprayed by high velocity oxygen fuel (HVOF) [18] or suspension plasma spray (SPS) [20]. However, studies report that using submicron feedstock, which it is possible in the SPS process, can further enhance the tribological performance of thermally sprayed ceramic coatings [21,22].

Therefore, this study aims to compare a thermally sprayed CoO coating with two widely used alloys in the aero-engine sector (i.e., Haynes 25 and Inconel 718) in terms of wear and friction and identify the compounds formed at the interface after the tests. The CoO coating was applied using suspension plasma spray technique over Inconel 718 substrates, and the surfaces were tested at 600 °C and 800 °C using a ball-on-flat tribometer setup, with Inconel 718 serving as the counterface. Focused ion beam (FIB) cross-sections of areas of interest were examined to gain a deeper understanding of the tribofilms formed during testing. Ex-situ analyses of the tribofilms were conducted using Raman spectroscopy and X-ray photoelectron spectroscopy (XPS) to identify the compounds formed at the interface and to provide insights into the wear mechanisms.

2. Materials and methods

The cobalt (II) oxide coating was sprayed using suspension plasma spray technique. The coatings were deposited on Inconel 718 softened annealed (McMaster, USA) using a Mettech's Axial III plasma spray system with the parameters shown in Table 1. Substrates with dimensions of 25 x 25 × 7 mm were grit blasted using alumina in a size of 80 mesh to achieve a desired roughness and cleaning the surface before spraying. The feedstock was a suspension with 20 wt% of solid content that was prepared using ethanol as the base and 1 wt% (in relation to the solid content) of PVP (Polyvinylpyrrolidone) as a dispersant agent. More detailed information on how to prepare the suspension and characterization of the powder is available elsewhere [20].

Scanning electron microscopy (SEM) images were performed using a S-3400 while Field Emission Scanning Electron Microscopy (FE-SEM) was performed using a SU8200 (Hitachi, Japan), in both cases an energy dispersive X-ray detector (Oxford, UK) was used. A 532 nm wavelength inVia Raman system (Renishaw, UK) with a Leica microscope equipped with a 50x objective lens was used to acquire the Raman spectra of the coatings and wear tracks. Vickers micro-hardness was performed using an MFT-5000 (RTec, USA) equipped with an instrumented indentation tester module. A total of 9 indentations for each material was performed with a load and unload rates of 10 μm/min, a holding time of 15 s, and a maximum applied force of 2 N. The load-displacement curves were analyzed using the Oliver and Pharr method to calculate the hardness values [23]. A calibration using a fused quartz reference material was performed; this method was chosen to account for tip roundness and ensure accuracy in measurements, particularly given the relatively small displacements during the hardness tests. X-ray diffraction was performed using a D8 Advance X-ray diffractometer (Bruker, Germany) using a Cu-Kα ($\lambda = 1.54$ Å) source. X-ray photoelectron spectroscopy (XPS) analyses were performed using a PHI 5000 VersaProbe II (Ulvac-PHI Inc., USA). The X-ray beam from the Al Kα target was focused on a 200 μm diameter spot on the surface. Focused ion beam (FIB) was performed using a Helios NanoLab DualBeam 650 (Thermo-Fischer Scientific, USA). The cuts were made with dimensions of 30 × 12 × 18 μm, and images were taken at a tilt angle of 52°.

A POD 4.0 DUCOM tribometer (Ducom Instruments, USA) was used to measure the coefficient of friction by ball-on-flat reciprocating tests. For each condition a total of three tests were performed in angular oscillation mode at 1 Hz, with a track diameter of 10 mm and angle of 30°, resulting in an average speed of 5.2 mm s^{-1}. The friction results were reported as average curves with standard deviation bars. A relatively low speed for the reciprocating motion was chosen in order to induce the formation of a glaze layer on the metallic samples, as observed by Stott [24]. The tests were performed at 600 °C and 800 °C on surfaces polished with 3 μm diamond suspension, achieving a mirror finish free of scratches. The tested samples included Inconel 718 in a softened annealed condition (McMaster, USA), Haynes 25 in a solution annealed condition (HPAlloy, USA), and a thermally sprayed CoO coating. The samples were heated from room temperature to the target temperature, taking approximately 25 min to reach 600 °C and 50 min to reach 800 °C. The target temperature was maintained for an additional 15 min before testing to ensure a uniform temperature distribution. Each test consisted of 7200 cycles, corresponding to a total testing duration of 2 h. After testing, the samples were cooled to room temperature inside the furnace with the lid open. Surface analysis was performed using a Lext laser microscope OLS4100 (Olympus, Japan). For roughness measurements, three different areas measuring 1.2 × 1.2 mm were analyzed, and the results were reported as their average. Optical microscopy was also carried out using the Lext microscope (Olympus, Japan). Inconel 718 balls (RGP Balls, Italy) with 10 mm in

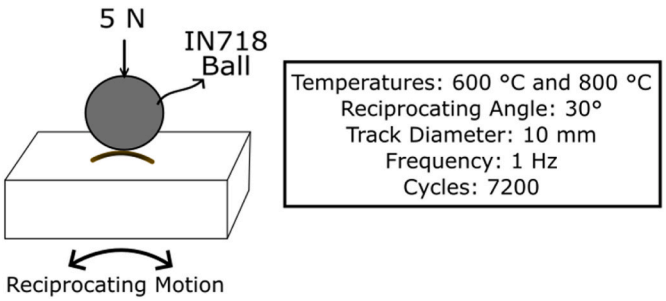

Fig. 1. Tribological test parameters.

diameter were used as counterface and a force of 5 N was applied. The wear of the counterfaces was calculated using ASTM G133. The schematic below, Fig. 1, represents an overview of the test.

3. Results

3.1. Characterization

Table 2 shows the chemical composition of the materials studied. The Inconel 718 and Haynes 25 materials presented a chemical composition consistent with values reported in the literature [25–27]. For the CoO coating, a small oxygen deficiency is observed. Fig. 2 shows SEM images of the materials used in this study. Based on Fig. 2(a and b), it is possible to observe the presence of carbides within the Inconel 718 counterfaces and Inconel 718 flat surfaces. In the case of the counterfaces, Fig. 2(a)–a different morphology was observed when compared to the Inconel 718 plate, Fig. 2 (b), without visible grains. For the Haynes 25, Fig. 2 (c), the presence of twinning alongside tungsten-rich precipitates is visible, as also observed in other studies [27,28]. The thermally sprayed CoO coating, Fig. 2 (d), shows a dense morphology with the presence of few vertical cracks. At higher magnification, shown in the inset, it is possible to observe the presence of small pores and lamellas of metallic cobalt. The presence of metallic cobalt is discussed in a previous study [20].

A more detailed analysis of the precipitates is present in Fig. 3. For Inconel 718, from both the counterfaces and flat surfaces, shown in figures Fig. 3(a and b), carbide phases rich in Nb and of similar composition were observed, which are commonly reported for such alloys [25,29]. On the counterface, Fig. 3 (a), an MN-nitride phase was also identified, consistent with findings for this alloy in other studies [30]. In the case of Haynes 25, Fig. 3 (c), precipitates in the form of MC-carbide phases rich in W, Co, and Cr were observed.

The hardness of the samples is present in Table 3 and the load-displacement curves in Fig. 4. A higher hardness was observed in the counterfaces compared to the Inconel 718, as result from different morphology, as shown in Fig. 2. Some pop-ins were observed in the Inconel 718, as shown in Fig. 4, which is a characteristic of dislocation nucleation events and has also been previously observed in other nickel-based alloys [31]. The Haynes 25 presented a slightly higher hardness compared to the Inconel 718, with the highest hardness observed by the thermally sprayed CoO coating.

Table 2
Chemical composition of the materials studied measured by EDX.

Nickel-based	Ni (wt%)	Fe (wt%)	Cr (wt%)	Nb (wt%)	Mo (wt%)	Ti (wt%)	Al (wt%)
Inconel 718 (Counterfaces)	52.1 ± 0.2	19.7 ± 0.2	17.9 ± 0.02	5.9 ± 0.1	3.0 ± 0.1	1.0 ± 0.1	0.5 ± 0.1
Inconel 718	51.3 ± 0.7	18.9 ± 0.4	18.6 ± 0.1	6.2 ± 0.9	3.3 ± 0.2	1.2 ± 0.02	0.5 ± 0.1

Cobalt-based	Co (wt%)	Cr (wt%)	W (wt%)	Ni (wt%)	Fe (wt%)	Mn (wt%)
HS25	49.1 ± 0.1	20.5 ± 0.03	16.7 ± 0.4	9.8 ± 0.1	2.4 ± 0.2	1.6 ± 0.2

Coating	Co (wt%)	O (wt%)	Co (at%)	O (at%)
CoO	79.6 ± 0.3	20.4 ± 0.3	51.4 ± 0.5	48.6 ± 0.5

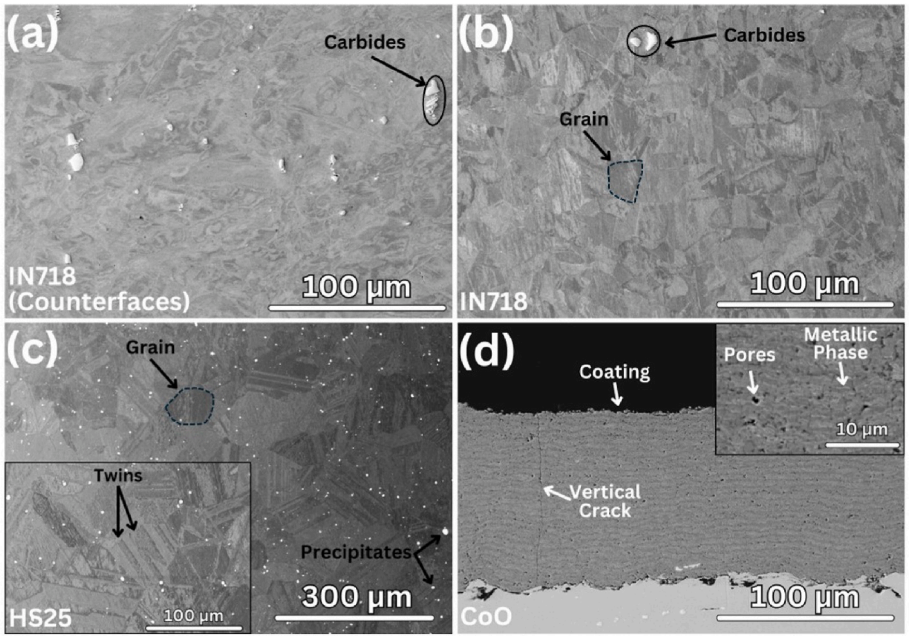

Fig. 2. SEM images of the microstructure of the (a) counterfaces, (b) Inconel 718, (c) Haynes 25, and the cross-section of the (d) CoO coating.

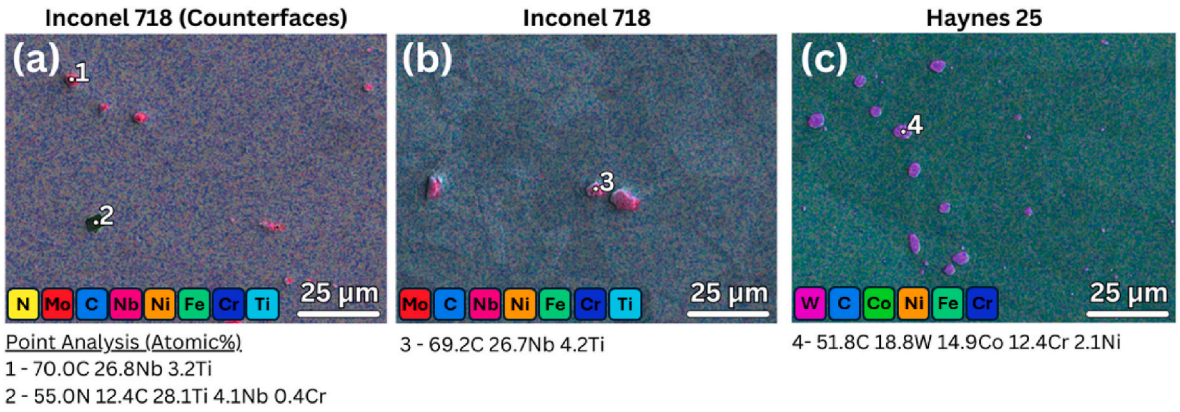

Fig. 3. FE-SEM images overlapped with EDX mapping images and points analysis of the (a) counterfaces, (b) Inconel 718, and (c) Haynes 25.

Table 3
Measured hardness of the surfaces studied.

Sample	Hardness (GPa)
Counterface	4.4 ± 0.6
Inconel 718	2.4 ± 0.5
Haynes 25	3.2 ± 0.2
CoO coating	5.2 ± 0.8

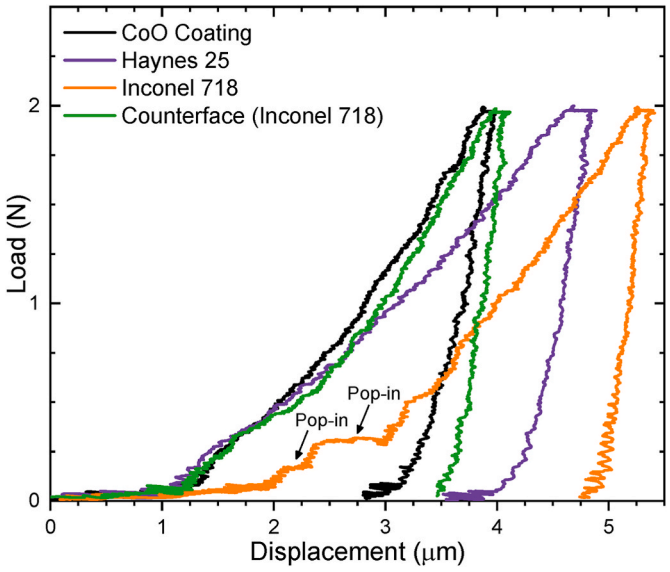

Fig. 4. Load-displacement curves of the surfaces studied.

Fig. 5 shows the XRD analysis of the CoO coating and the alloys tested. The Haynes 25 and Inconel 718 presented a face-centred cubic (FCC) arrangement, typical for these alloys [26,27,32,33]. In the specific case of the CoO coating, alongside the peaks relative to the cobalt (II) oxide, a small peak of metallic cobalt was also observed. This is due to the metallic phase observed on the cross section, shown in Fig. 2 (d) inset and observed in a previous study [20].

3.2. Tribological Evaluation

Fig. 6 shows the coefficient of friction for the surfaces tested against Inconel 718 counterfaces at two different temperatures. At 600 °C, a slight difference in the coefficient of friction was observed during the steady state, with the metallic alloys exhibiting slightly lower values. At 800 °C, the different surfaces displayed similar coefficients of friction

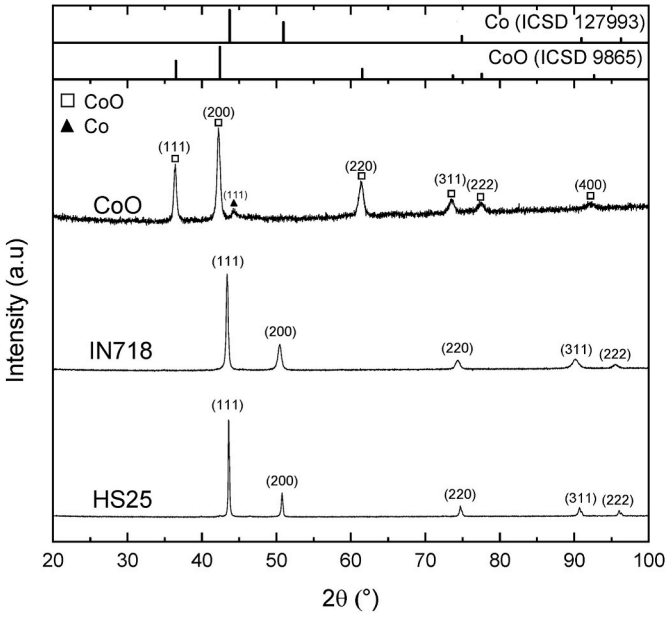

Fig. 5. X-ray diffractogram of the coating and alloys.

after reaching steady state. Despite the similar friction values, the break-in periods varied significantly. At both 600 °C and 800 °C, Inconel 718 required more cycles to reach a steady state coefficient of friction, whereas Haynes 25 and the CoO coating achieved steady state with fewer cycles and a smoother transition.

Fig. 7 shows the wear tracks formed on the flat surfaces after the ball-on-flat tests, while Table 4 presents the chemical composition of the analyzed regions, acquired by EDX, in atomic percentages. For the CoO coating, the major difference observed between 600 °C and 800 °C is the presence of abrasion grooves at the higher temperature. Additionally, a small amount of nickel from the counterface was transferred into the coating surface, as indicated in Table 4. For Haynes 25, oxide isles (i.e., a partially formed and uneven glaze) were present at 600 °C, with a homogeneous oxide layer (i.e., glaze layer) formed at 800 °C. However, the analysis of these oxides by EDX revealed similar chemical compositions at both temperatures, with a high percentage of nickel present in both cases. For Inconel 718, oxide isles were also observed at 600 °C, but these did not further develop into glaze layers at 800 °C.

Fig. 8 shows optical microscopy images along with their corresponding 3D topography. For the CoO coating, a narrower wear track was observed at 600 °C compared to the metallic surfaces. The 3D images also reveal a homogeneous and mild wear pattern after testing. In contrast, the metallic surfaces exhibited a more heterogeneous wear

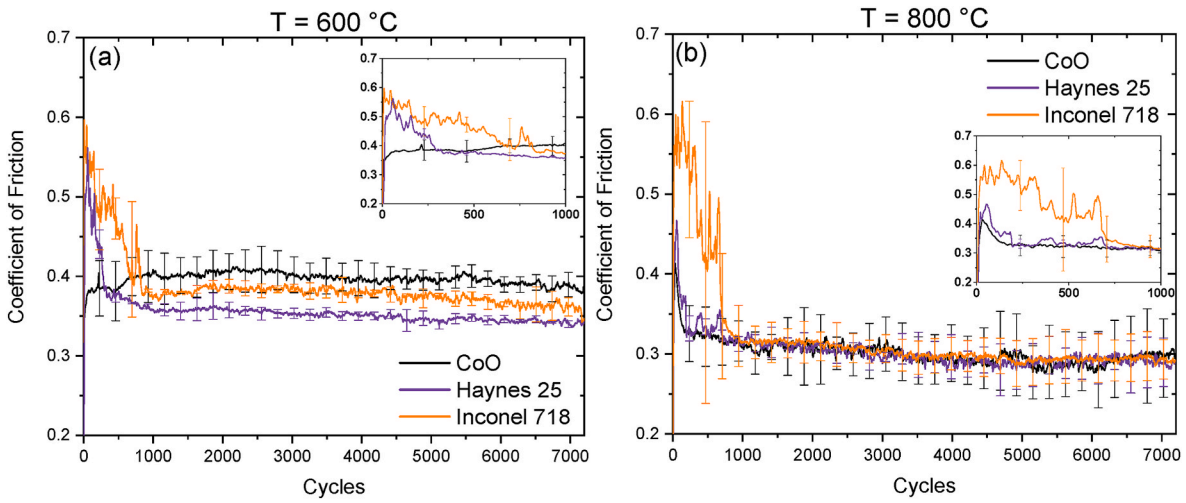

Fig. 6. Average coefficient of friction at (a) 600 °C and (b) 800 °C versus Inconel 718 counterfaces.

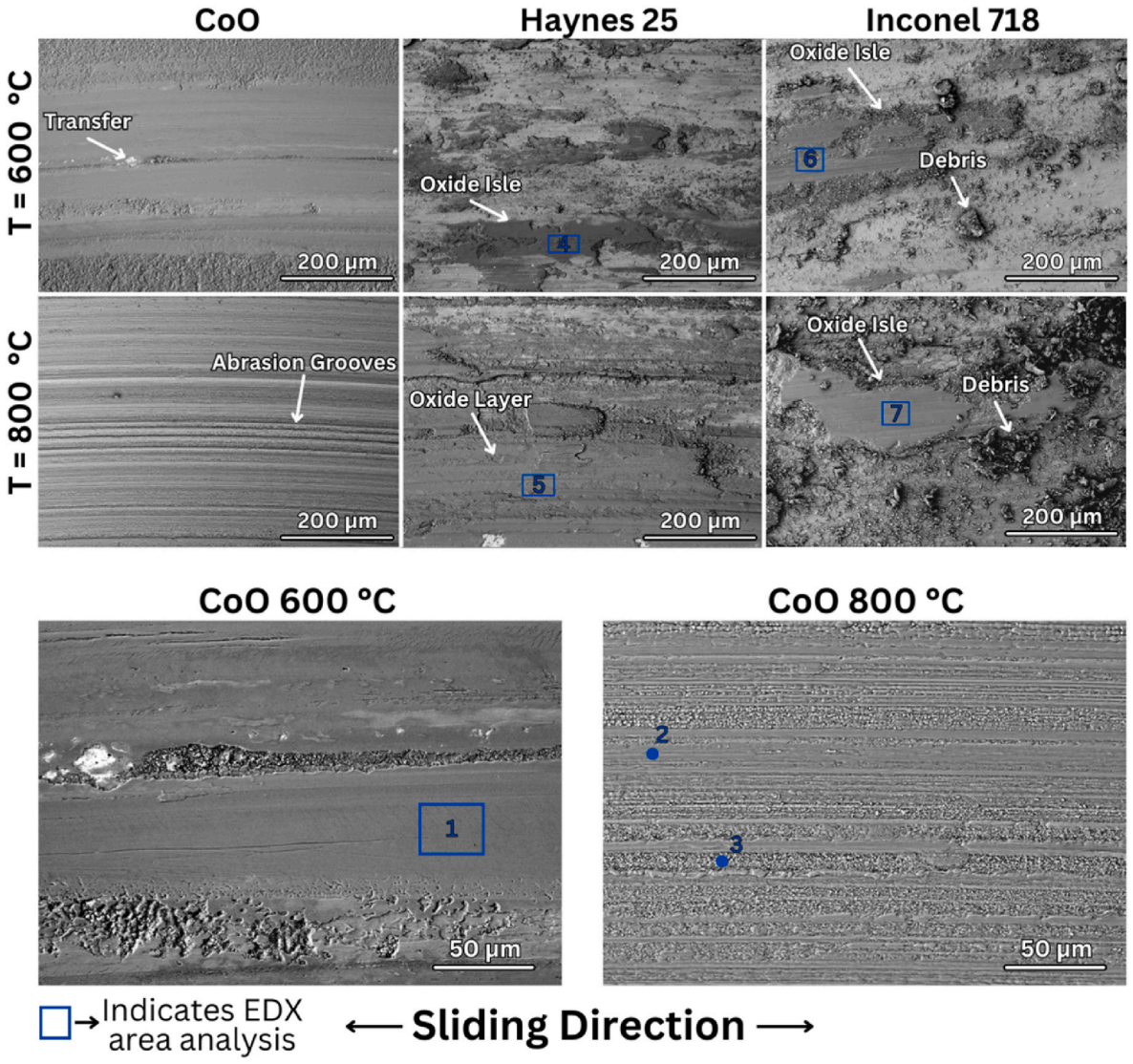

Fig. 7. SEM images of the wear tracks. Numbered box indicates the position where EDX analysis was performed.

Table 4
EDX analysis of the flat surfaces shown in Fig. 7.

	Spectrum	O	Ni	Fe	Cr	Co	[a]Others
CoO	1	56.7	4.9	1.7	1.9	34.8	0
	2	60.4	0	1.2	1.1	37.4	0
	3	60.2	3.9	0.9	1.0	34.0	0
HS 25	4	58.7	17.5	7.8	7.7	6.5	1.8
	5	59.2	18.7	7.5	8.6	4.3	1.7
IN 718	6	50.7	25.6	8.6	11.2	0	3.9
	7	56.5	20.2	13.8	8.1	0	1.4

[a] Minor percentages of Al, Nb, Ti, and W.

track at the same temperature. At 600 °C, Haynes 25 and Inconel 718 showed the formation of some oxide isles. The topography indicates that minimal wear occurred in these regions. At 800 °C, some differences were observed. The CoO coating displayed a slightly wider wear track. The Haynes 25 showed a substantial increase in oxide formation, leading to the development of a glaze layer on the surface. In contrast, Inconel 718 exhibited only a few isolated oxide spots at this temperature.

The combined wear volume is shown in Fig. 9. For the CoO coating, a minor difference in wear volume was observed with the change in temperature; however, an increase in counterface wear was noted. For Haynes 25, the formation of the glaze, shown in Fig. 8, substantially decreased the wear of the flat surface and counterface. For Inconel 718, no substantial difference in total wear was observed with the increase in temperature, although the distribution of total wear shifted. It can be observed that, despite a slight increase in the average combined wear volume (i.e., counterface plus flat surface wear), there was a significant decrease in counterface wear.

Fig. 10 shows the SEM images of the counterfaces, while Table 5 presents the chemical composition acquired by EDX in atomic percentages for the analyzed regions. At 600 °C, a substantial wear scar was observed for Haynes 25 and Inconel 718, whereas a significantly smaller

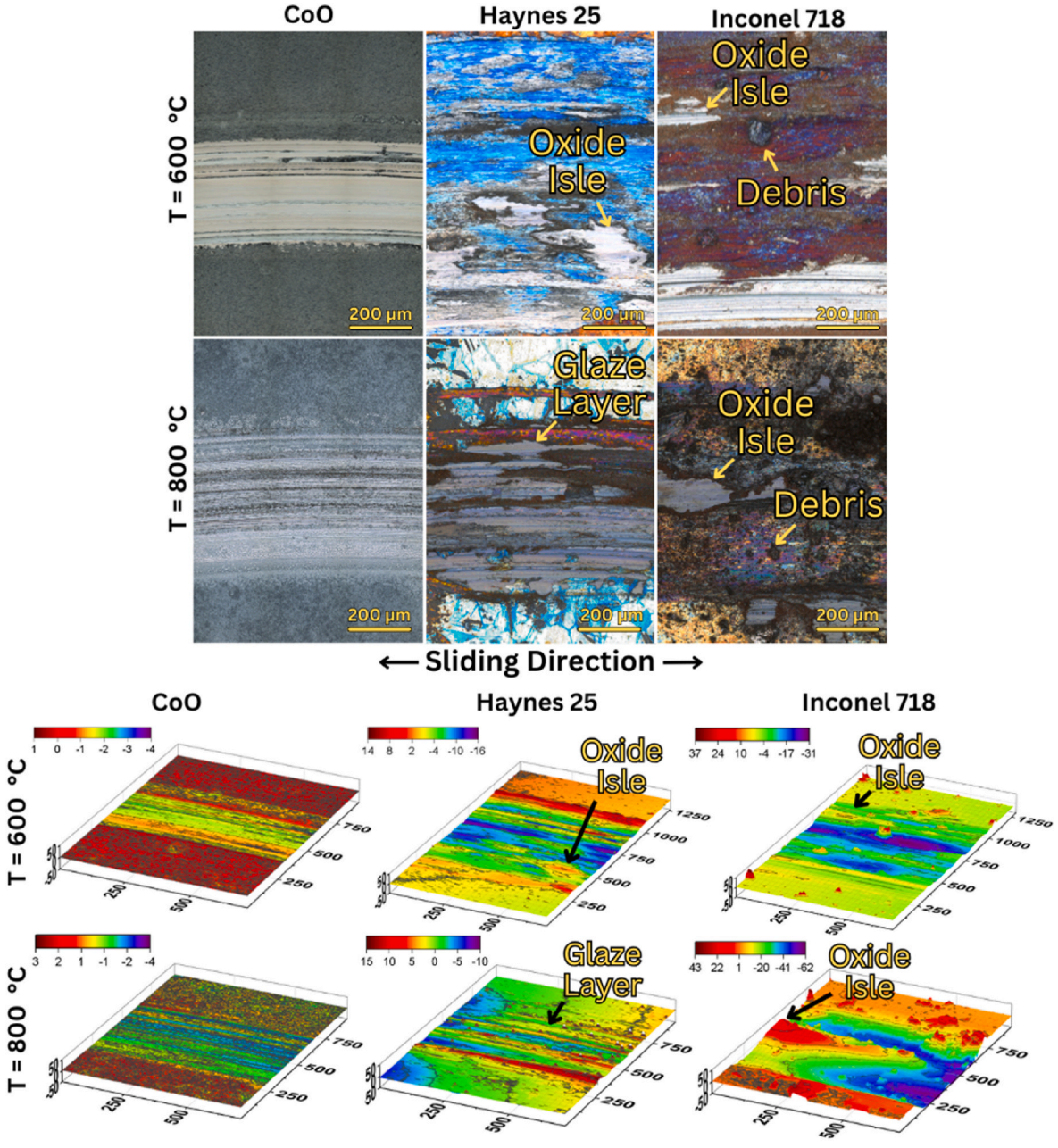

Fig. 8. Optical microscopy images and surface topographies of the wear tracks at different temperatures.

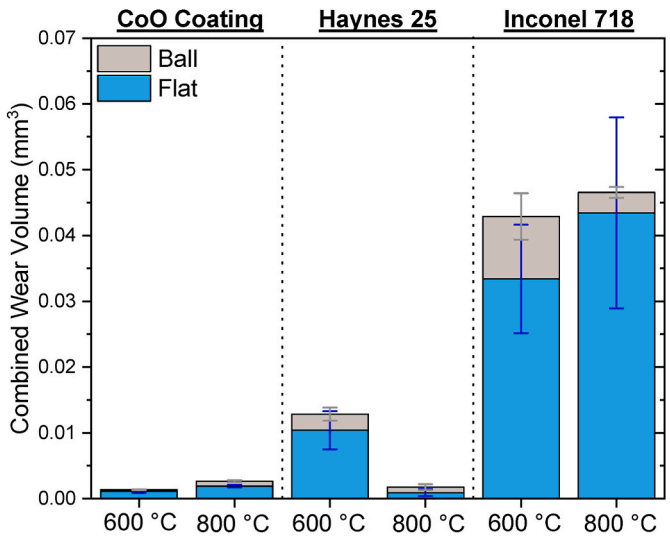

Fig. 9. Combined Wear Volume (i.e., flat surface plus counterface) after ball-on-flat tests.

wear scar was observed for CoO. For the counterfaces tested against the metallic materials at 600 °C, a well-distributed oxide layer was observed, while for CoO, localized regions covered by oxides were observed. Additionally, the cobalt content on the counterface tested against the CoO coating, as shown in Table 5, indicates that this oxide layer is primarily formed through material transfer from the coating. At 800 °C, a decrease in the counterface wear scar size was observed when tested against Haynes 25 and Inconel 718. However, the opposite trend was observed for the CoO coating. At this temperature, much less cobalt transfer was observed on the counterfaces tested against CoO and Haynes 25, with a substantial decrease for the CoO coating and no cobalt detected for Haynes 25, as shown in Table 5.

To further understand the nature of the oxides formed at the interface, Raman spectroscopy was performed, and the results are shown in Fig. 11. For the CoO coating, Co_3O_4 was observed at both temperatures, originating from the oxidation of the coatings, with similar peak positions also observed by Rivas-Murias and Salgueiriño [34]. A spinel peak was also detected at the CoO wear track at 600 °C. For Haynes 25, spinels were observed at both temperatures. However, a more pronounced peak related to Cr_2O_3 at around 550 cm^{-1} was detected at lower temperatures, with this peak position also reported as Cr_2O_3 by other studies [35,36]. Additionally, a peak related to CoO was found at lower temperatures, however, similar peak position was also observed for NiO [37]. Among the spinels, Co_3O_4 is possibly present, but due to the proximity of the peaks, accurate deconvolution for spinel structures is challenging. Similar peak positions are reported in the literature [38–40] and the possibility of solid solution formation among them [41]. For Haynes 25 at 800 °C, the observed peaks are similar to those reported by Kim and Koh [39], suggesting the formation of nickel-cobaltite ($Ni_xCo_{3-x}O_4$). NiO oxide was also observed at 800 °C, with similar peaks documented in the literature [37,42]. For Inconel 718, peaks related to spinels and NiO were observed at both temperatures. Additionally, a peak related to Cr_2O_3 was observed for Inconel 718 tested at 600 °C.

Oxidation of the surface, at the unworn region, was observed more severely on Haynes 25 at 800 °C and for the CoO at 600 °C and 800 °C. The oxidation effects on the surface of the CoO coating are shown in Fig. 12. It is possible to observe that different roughness is present accordingly to the temperature. However, when analyzing the surface by Raman it is possible to see that for both 600 °C and 800 °C sharp peaks related to Co_3O_4 are observed, while for the polished surface a spectrum for partially oxidized CoO is observed [34,43]. Fig. 13 shows the surface of the Haynes 25 after testing at 800 °C. Oxidation was observed to occur throughout the grains, as observed in Fig. 13. When analyzing the Raman spectrum in the middle of the grain, high intensity peaks related to Co_3O_4 were also observed. However, differently to the CoO coating, a small shoulder next to the A_{1g} peak was observed, which could indicate the presence of other oxides.

3.3. Cross sectional characterization

To further understand the formation of the tribofilms (e.g., glaze layer), more in-depth analyses were performed on Haynes 25 and the CoO coating surfaces after testing at 800 °C. Fig. 14 shows cross-sectional focused ion beam (FIB) images of the CoO coating and Haynes 25. Larger grains were visible in the Haynes 25 sample, with the focused ion beam cut performed inside a grain, as shown by the inset in Fig. 13 (b). An oxidized layer was observed on both surfaces, as shown in Fig. 14(a and b), with the Haynes 25 showing different layers. When exposed to wear, shown in Fig. 14(c and d), the formation of a tribo-induced film with nanocrystalline grains was observed on both surfaces, corresponding to a 'glaze-layer'. For the CoO coating, a crystalline tribofilm was observed, with grain refinement underneath this layer. Additionally, smaller pores were observed underneath the wear track. In the case of Haynes 25, a layer of fine grains was observed underneath the glaze layer. No grains were detected in the glaze layer formed over Haynes 25, which is consistent with the amorphous nature of this type of glaze [44].

To better understand the different layers formed during the tribological tests, XRD and XPS sputter depth profile were performed, as shown in Fig. 15. For the CoO coating at the outside of the wear track, XRD was used to observe the formation of Co_3O_4 by the oxidation of the coating, as CoO and Co_3O_4 show similar spectra when analyzed by XPS [45], making their differentiation challenging. The XRD spectrum for the unworn CoO, as shown in Fig. 15 (a), exhibits the presence of Co_3O_4 caused by oxidation during the test and CoO from underneath the oxidation layer. Inside of the wear track of the CoO coating, Fig. 15 (c), the presence of nickel and chromium was observed. For the Haynes 25 at the unworn region, Fig. 15 (b), a change in concentration of elements was observed, corroborating with the two different zones observed in Fig. 14 (b). Two different cobalt species were observed, suggesting different oxidation states in the different layers. In the worn region, Fig. 15 (d), a homogeneous chemical composition was observed at the first 750 nm for the major concentration elements. Subsequently, an increase in metallic cobalt was observed with the decrease in oxidized cobalt. A similar composition was observed by EDX, as shown in Table 4. However, due to peak overlap the concentration of iron was not possible to be precisely defined by XPS. Also, similarly to the metallic cobalt, an increase in metallic tungsten was observed, as shown in Fig. 15 (d).

4. Discussion

4.1. Friction and wear

As shown in Fig. 6, similar coefficient of friction values for the surfaces analyzed were observed. However, at 600 °C a slightly higher coefficient of friction for the CoO coating was observed when compared to the Haynes 25 and Inconel 718. The major difference observed in terms of friction was the break-in period. A comprehensive review on the morphology of those curves was performed by Peter J. Blau [46]. For the CoO coatings, at both temperatures, the break-in period was relatively short, and the coefficient of friction achieved steady state quickly. However, at 600 °C a small increase in the coefficient of friction is observed in the first stages and the sample achieves steady state quite quickly. At 800 °C, the CoO coating shows opposite trend, lowering the coefficient of friction at the first stages. This could be caused by the rougher oxidized surface formed during the exposition to high temperature. It is possible to observe on Fig. 14 (a) the formation of an oxidation layer on top of the coating. It should be noted that even the

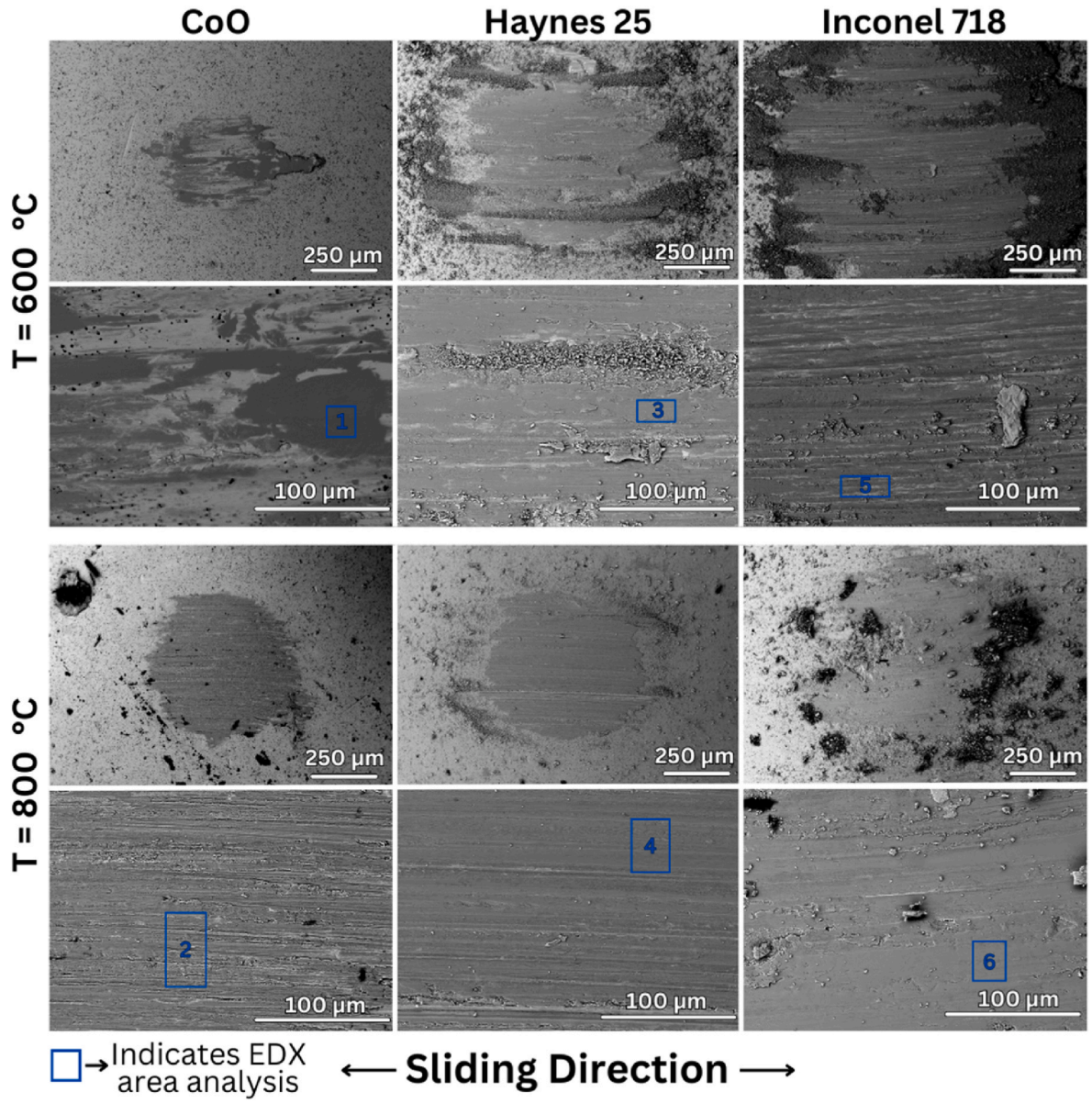

Fig. 10. SEM images of the counterfaces. Numbered box indicates the position where EDX analysis was performed.

Table 5
EDX analysis of the counterfaces shown in Fig. 10.

	Spectrum	O	Ni	Fe	Cr	Co	[a]Others
Versus CoO	1	58.8	1.4	0.6	0.8	38.4	0
	2	51.2	23.4	8.8	11.6	5.1	0
Versus HS 25	3	55.8	16.3	6.2	8.6	12.3	0.9
	4	57.7	22.2	8.9	8.5	0	2.7
Versus IN 718	5	51.3	26.1	10.1	10.2	0	2.4
	6	57.8	22.1	11.0	7.1	0	2.0

[a] Minor percentages of Al, Nb, and Ti.

samples being polished before the tests, this layer was formed on the unworn surface (i.e., subsequently to the high temperature exposure) caused by oxidation from CoO to Co_3O_4, as observed in the Raman spectra and SEM images of the surfaces in Fig. 12. For the metallic surfaces (i.e., Haynes 25 and Inconel 718) in both cases a reduction in coefficient of friction was observed. This is due to the formation of the oxides during the transient period, as observed in the previous ex-situ analyses. These oxides can create a barrier in metallic interfaces, reducing coefficient of friction and wear [47]. Also, it was observed a similar behaviour in terms of friction and break-in period for the CoO coating and Haynes 25 at 800 °C. Indeed, both of these systems have shown to form Co_3O_4 during the oxidation, as shown in the top surface in Figs. 12 and 13 and by the cross section in Fig. 14, therefore presenting similar surfaces during the initial stages of the test.

Compared to metallic materials, the CoO coating exhibited only a slight increase in wear with rising temperatures, as shown in Fig. 9. Conversely, for Haynes 25, a decrease in wear was observed as the temperature increased. The primary reason for this was the formation of oxides at the interface, as observed in Fig. 8. With the increase in temperature, a well-structured glaze layer formed on the wear track, significantly reducing wear. The formation and major characteristics of the glaze is well described by Viat et al. [44]. In contrast, Inconel 718 exhibited the highest wear among the materials tested. At both temperatures, Inconel 718 took the longest time to reach a steady state, possibly resulting in high amounts of wear. Additionally, even at 800 °C, the oxides formation on the track surface was inconsistent, leading to significant variation among the tested samples.

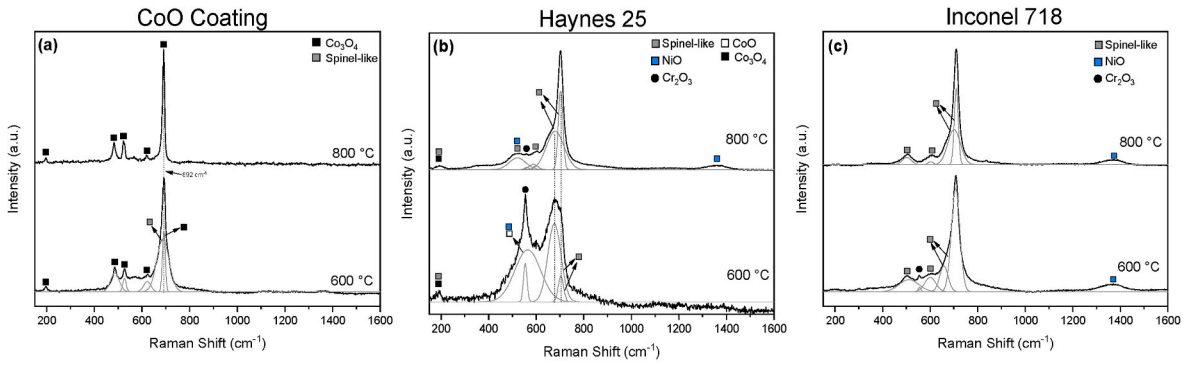

Fig. 11. Raman spectra for (a) CoO coating, (b) Haynes 25, and (c) Inconel 718 at the wear track.

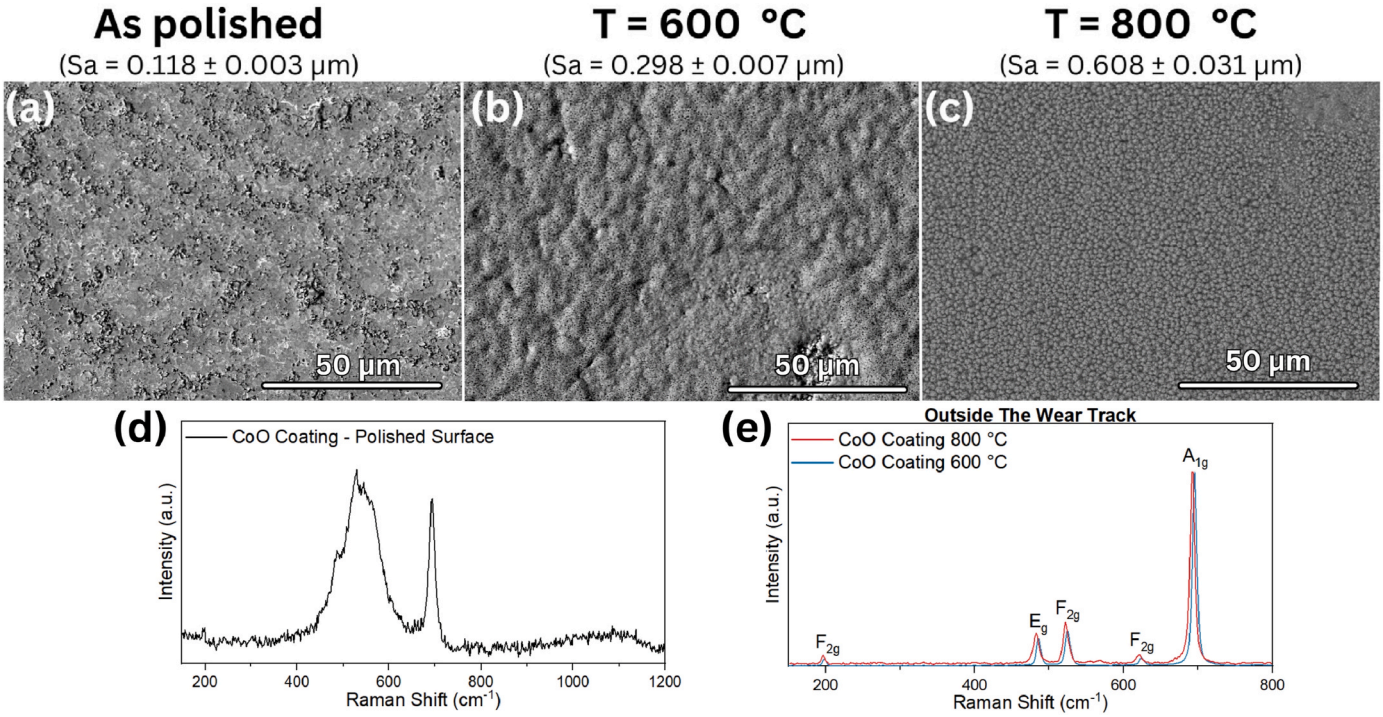

Fig. 12. Images of the CoO coating outside the wear track: (a) FE-SEM of the as-polished surface, and SEM after ball-on-flat tests at (b) 600 °C and (c) 800 °C, along with their Raman spectra (d, e).

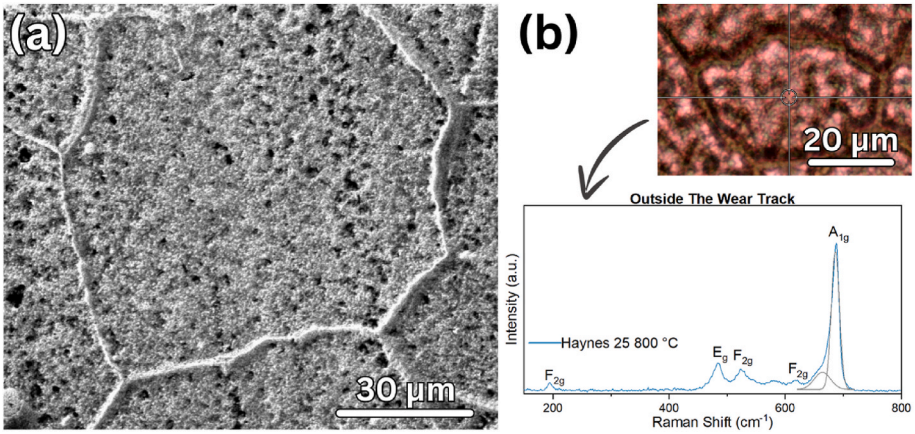

Fig. 13. Haynes 25 in the unworn region after tests at 800 °C. (a) SEM image of the surface, and (b) optical microscope image acquired alongside its Raman spectra. The target at the center indicates the position where the Raman spectrum was performed.

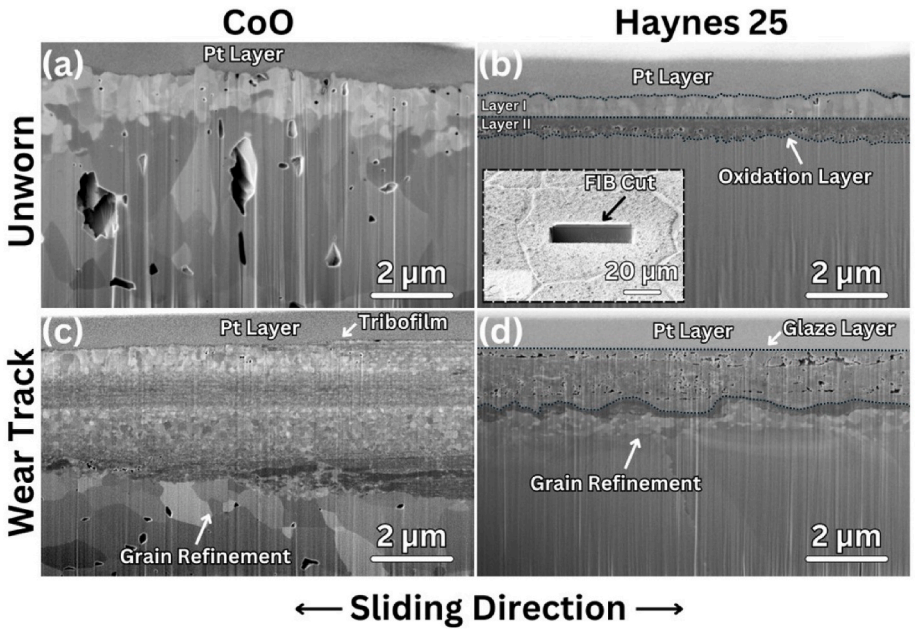

Fig. 14. SEM images from FIB cuts at (a, b) unworn and (c, d) wear tracks of the CoO coating (a, c) and Haynes 25 (b, d) tested at 800 °C.

SEM analysis, shown in Fig. 7, along with the chemical composition data in Table 4, revealed further details. At 600 °C a smooth surface was observed inside the wear track for the CoO coating, whereas at 800 °C the presence of grooves characteristic of abrasion was observed. Nickel incorporation from the counterface was also observed, as indicated in Table 4. For Haynes 25, smooth oxide layers were observed at both temperatures, with similar chemical compositions, showing high levels of nickel from the counterface. This suggests that the glaze formation originated from debris particles from both, Haynes 25 and the counterface (Inconel 718). Similarly, oxides were observed for the Inconel 718 flat surface. However, these oxides were more unevenly distributed throughout the wear track, as also observed in Fig. 8, creating less protection of the surface and leading to more wear.

When examining the counterfaces, Fig. 10, at 600 °C, the wear scar when testing against the CoO coating was minimum. However, the oxide distribution was uneven, with spots showing large amounts of cobalt, as present in Table 5. At 800 °C, the wear scar on the counterface increased in size, and cobalt presence in the EDX analysis decreased. A similar reduction in cobalt adhesion to the counterfaces at 800 °C was observed for samples tested against Haynes 25. For Haynes 25, a decrease in counterface wear was noted, with values comparable to those of the CoO coating, Fig. 9. In the case of the Inconel 718, the wear scar of the counterface also decreased by the increase in temperature and a more homogeneous layer of oxide was observed at the counterface.

4.2. Composition and distribution of oxides at interfaces

To further increase the understanding of the compounds formed in the interface during the tribological tests, Raman Spectroscopy was performed. As shown in Fig. 12, a change in the oxidation state of the cobalt oxide coating was observed. This oxidation transformed the CoO present in the coating, as observed by XRD analysis in Fig. 5, into Co_3O_4. This oxidation is expected to happen, as also observed by Tomlinson and Easterlow under similar temperatures [48]. Indeed, when analyzing the compounds observed in the interfaces after the tests, Fig. 11, peaks related to Co_3O_4, well stablished in the literature [49], are observed for the CoO coating at both 600 °C and 800 °C. This spinel form of cobalt oxide is found in the glaze layers of cobalt-based alloys [10,44] and deemed as the major component of these layers. At lower temperatures, a broad peak at around 692 cm^{-1} was also observed, suggesting an overlapped peak of Co_3O_4 with other spinels forms (e.g., $NiCo_2O_4$, $CoCr_2O_4$, among others). However, crystallinity changes formed over the surface, alongside crystal defects, such as vacancies, could also cause the Raman spectra to change [50].

For the Haynes 25, distinct spectra were observed at the different temperatures. At 600 °C a protruding peak related to chromium oxide was observed among a mixed signal with CoO and spinel-like compounds, and a formation of a glaze layer was not observed. At 800 °C tough, a more protruding peak at 704 cm^{-1} was observed alongside other oxides, and the formation of a glaze observed. For the Inconel 718, similar spectra were observed at both temperatures, with the major difference of a peak related to Cr_2O_3 at 600 °C. Due to the possibility of forming different types of spinels, with the possibility of solid solution [25], and a mixed chemical composition, observed in Table 4, the exact chemistry of the spinels found in the interfaces cannot be determined. Also, the peaks around 700 cm^{-1} have presented a shoulder (i.e., a smaller intensity overlapped peak), commonly observed by Hosterman when studying the solid solution of spinel oxides [41].

Due to the complexity of the compounds observed at the interfaces, a few conditions were selected to perform FIB cross section and XPS analysis. In the case of the CoO coating a thin layer of fine Co_3O_4 grains was observed at the top of the coating, shown in Fig. 14 (a). Similarly, Haynes 25 showed an oxidation layer on the unworn surface, presenting two different layers, shown in Fig. 14 (b). In both cases, the oxidation process has created a Co_3O_4 layer, causing similar friction during the break-in period at such temperatures. In the specific case of Haynes 25, the composition of this glaze drew attention due to the high amount of nickel, as observed in Table 4. To further understand the chemical composition of the interfaces, XRD and XPS sputter depth profile were performed, as shown in Fig. 15. The CoO coating has shown the presence of Co_3O_4, shown in Fig. 15 (a), which was expected based on the previous Raman analysis. When analyzing its depth profile at the wear track, Fig. 15 (c), a small portion of nickel and chromium was observed, originated from mechanically mixing with the counterface. Nonetheless, minimal changes were observed throughout the profile, with decrease in the amounts of nickel and chromium, suggesting only small differences in chemical composition between the layers observed in Fig. 14 (c).

For the Haynes 25 in the unworn region, Fig. 15 (b), the first layer showed a chemical composition composed of mostly cobalt oxide with traces of nickel (≈ 5 at%). When performing top analysis by Raman,

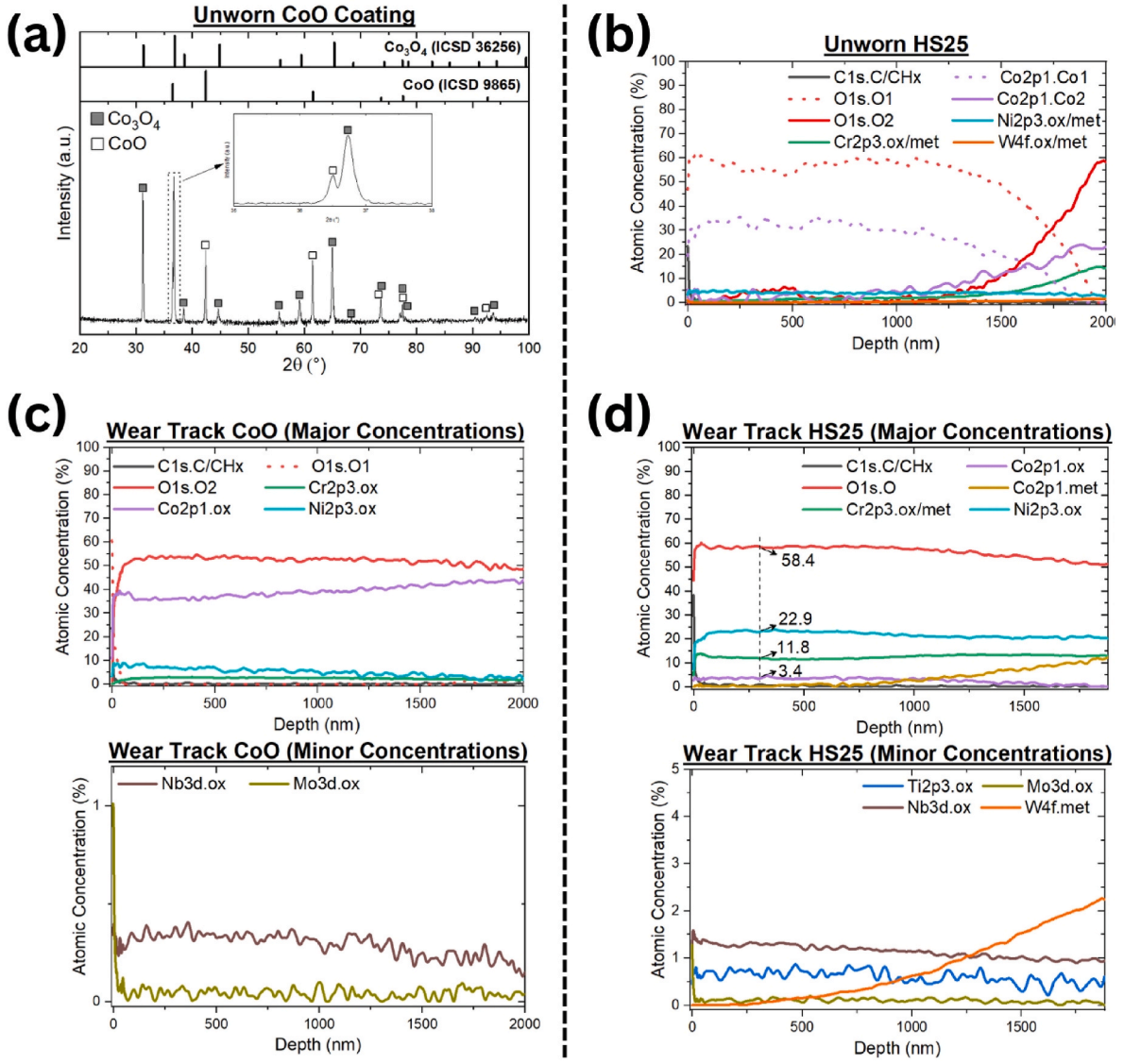

Fig. 15. (a) X-ray diffractogram and (b–d) XPS sputter depth profile of CoO coating and Haynes 25 tested at 800 °C. (a–b) Unworn and (c–d) wear track regions.

Fig. 13 (b), it was observed a spectrum related to Co_3O_4 with the presence of a shoulder in the A_{1g} peak. A similar shoulder was observed by Qi et al. when analyzing nickel-doped Co_3O_4 ($Ni_{0.2}Co_{2.8}O_4$) [51]. After approximately 1250 nm in depth, the composition starts to change due to the presence of a secondary layer, as observed in Fig. 14 (b). This second layer exhibited a mixed composition, primarily consisting of cobalt, chromium, and nickel, at both oxidized (predominantly) and metallic states. In the worn region, Fig. 15 (d), a chemical composition similar to those obtained by EDX was observed. Also, the presence of other minor concentration elements, such as titanium, niobium and molybdenum, alongside the depletion of cobalt indicates that the source of this nickel originates mostly from the counterface. However, the formation of a glaze layer was not possible when testing Inconel 718 at the same conditions. This result indicates that the small percentage of material originating from the Haynes 25 for the development of the glaze was fundamental for its formation.

4.3. Wear mechanism

The wear mechanisms observed on the CoO and Haynes 25 materials (i.e., low wear behavior) studied here are shown below in Fig. 16. Due to high temperatures, surface oxidation occurs through oxygen adsorption, leading to the formation of an oxide film. The nature of this oxidation depends on the chemical composition of the surface. This oxide layer is then mechanically removed by the counterface during sliding wear. However, during this process, wear of the counterface occurs, and debris from the counterface mixes into the surface. The extent of wear was found to be regulated by the amount of oxide formed on the surface; when only small amounts of oxide adhered to the surface, as in the case of Inconel 718, wear increased. In the specific cases of Haynes 25 and the CoO coating tested at 800 °C, grain refinement was also observed underneath the tribo-induced films.

5. Conclusions

A cobalt (II) oxide (i.e., CoO) coating was thermally sprayed and compared to two commonly used alloys in aerospace applications. After testing the surfaces at high temperatures under dry sliding conditions and analyzing their interfaces, a few conclusions can be drawn.

- The thermally sprayed CoO coating demonstrated improved wear resistance comparable to that of Haynes 25. The CoO coating exhibited similar wear and friction in conditions where a glaze layer was observed on Haynes 25 and significantly better wear resistance

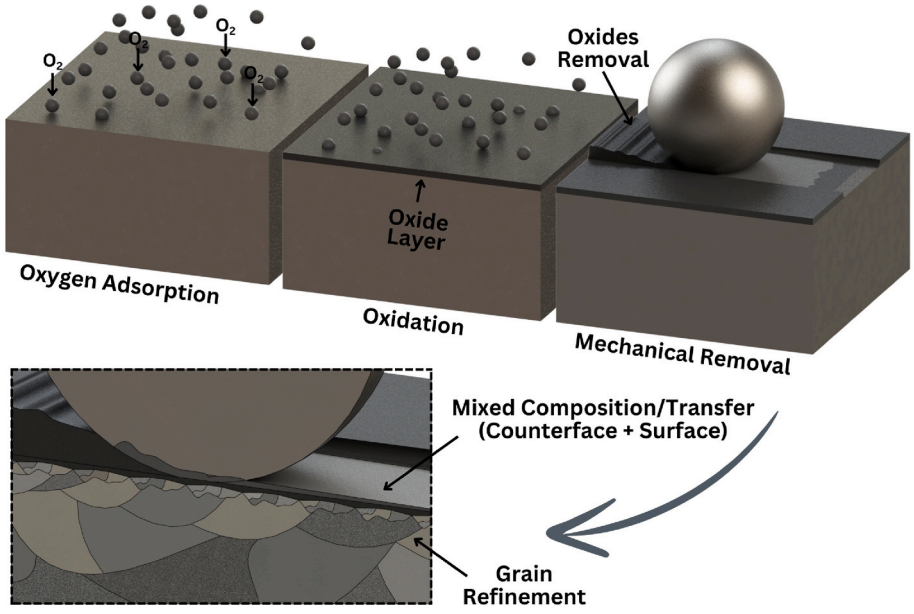

Fig. 16. Proposed wear mechanism for the tested low wear behavior surfaces.

when Haynes 25 was unable to stabilize a glaze. Additionally, wear on the counterface was minimal when tested against CoO, making these coatings an excellent choice for protecting the opposing surface in tribological interfaces.

- Both the CoO coating and Haynes 25 formed a layer based on Co_3O_4 on the surface at 800 °C, which played an important role during the break-in period. While the CoO coating did not show significant material transfer from the counterface into the tribofilm, the glaze layer observed on Haynes 25 contained a substantial portion of material originating from the counterface. Even under favorable conditions for glaze layer formation (i.e., low reciprocating speed at high temperatures), only the Haynes 25 at 800 °C was capable of forming it among the metallic materials.
- Despite experiencing high overall wear, certain areas of the Inconel 718 alloy exhibited minimal wear. In these regions, oxide isles were observed. These oxides were able to mitigate wear in areas where their adhesion was maintained. However, even at the highest temperatures, these oxides were unable to sinter into a stable glaze layer.
- While the glaze layer formed on Haynes 25 at 800 °C originated from a mixture with the counterface with the presence a small percentage of cobalt, a glaze layer was not observed for Inconel 718 at same conditions. Therefore, despite the small concentration of elements originating from Haynes 25, its contribution was fundamental for the formation of a glaze layer.

Declaration of competing interest

The authors declare that they have no known competing financial interests or personal relationships that could have appeared to influence the work reported in this paper.

Acknowledgments

The authors gratefully acknowledge the financial support provided by the Natural Sciences and Engineering Research Council of Canada (NSERC) through the Alliance Grants program (ALLRP 571542 - 21) and by the Fonds de recherche du Québec – Nature et technologies (FRQNT) under the NOVA program

References

[1] J.H. Perepezko, The Hotter the Engine, the better, Science 326 (2009) 1068–1069, https://doi.org/10.1126/science.1179327.
[2] J. Zuidberg, Identifying airline cost economies: an econometric analysis of the factors affecting aircraft operating costs, J. Air Transport. Manag. 40 (2014) 86–95, https://doi.org/10.1016/j.jairtraman.2014.06.007.
[3] B. Graver, CO2 Emissions from Commercial Aviation, 2018, 2018.
[4] P. Stoyanov, K.M. Harrington, A. Frye, Insights into the tribological characteristic of Cu-based coatings under extreme contact conditions, JOM 72 (2020) 2191–2197, https://doi.org/10.1007/s11837-020-04087-7.
[5] C.T. Sims, A history of superalloy Metallurgy for superalloy Metallurgists, in: Superalloys 1984 (Fifth International Symposium), TMS, 1984, pp. 399–419, https://doi.org/10.7449/1984/Superalloys_1984_399_419.
[6] E.O. Ezugwu, Z.M. Wang, A.R. Machado, The machinability of nickel-based alloys: a review, J. Mater. Process. Technol. 86 (1999) 1–16, https://doi.org/10.1016/S0924-0136(98)00314-8.
[7] H. Kumar, P.K. Jain (Eds.), Recent Advances in Mechanical Engineering: Select Proceedings of NCAME 2019, Springer Singapore, Singapore, 2020, https://doi.org/10.1007/978-981-15-1071-7.
[8] K.M. Harrington, E.C. Miller, A. Frye, P. Stoyanov, Tribological insights of Co- and Ni-based alloys in extreme conditions, Wear 477 (2021) 203827, https://doi.org/10.1016/j.wear.2021.203827.
[9] A. Viat, A. Dreano, S. Fouvry, M.-I. De Barros Bouchet, J.-F. Henne, Fretting wear of pure cobalt chromium and nickel to identify the distinct roles of HS25 alloying elements in high temperature glaze layer formation, Wear 376–377 (2017) 1043–1054, https://doi.org/10.1016/j.wear.2017.01.049.
[10] A. Dreano, S. Fouvry, S. Sao-Joao, J. Galipaud, G. Guillonneau, The formation of a cobalt-based glaze layer at high temperature: a layered structure, Wear 440–441 (2019) 203101, https://doi.org/10.1016/j.wear.2019.203101.
[11] K. Luo, S. Li, G. Xu, S.R.E. Hosseini, J. Lu, Hot corrosion behaviors of directed energy deposited Inconel 718/Haynes 25 functionally graded material at 700 °C and 900 °C, Corros. Sci. 197 (2022) 110040, https://doi.org/10.1016/j.corsci.2021.110040.
[12] G.A. Campbell, The cobalt market revisited, Miner Econ 33 (2020) 21–28, https://doi.org/10.1007/s13563-019-00173-8.
[13] S. Van Den Brink, R. Kleijn, B. Sprecher, A. Tukker, Identifying supply risks by mapping the cobalt supply chain, Resour. Conserv. Recycl. 156 (2020) 104743, https://doi.org/10.1016/j.resconrec.2020.104743.
[14] M.M. Attallah, R. Jennings, X. Wang, L.N. Carter, Additive manufacturing of Ni-based superalloys: the outstanding issues, MRS Bull. 41 (2016) 758–764, https://doi.org/10.1557/mrs.2016.211.
[15] M.R. Dorfman, G. Dwivedi, C. Dambra, S. Wilson, Perspective: challenges in the aerospace Marketplace and Growth Opportunities for thermal spray, J Therm Spray Tech 31 (2022) 672–684, https://doi.org/10.1007/s11666-022-01351-x.
[16] J.T. DeMasi-Marcin, D.K. Gupta, Protective coatings in the gas turbine engine, Surf. Coating. Technol. 68–69 (1994) 1–9, https://doi.org/10.1016/0257-8972(94)90129-5.
[17] M. Asuquo, R.B. Nair, M. Fotoohinezhadkhales, A. Akbarnozari, P. Stoyanov, C. Moreau, Tribological behavior of Atmospheric plasma-sprayed Cu-Ni coatings, J Therm Spray Tech 33 (2024) 2447–2462, https://doi.org/10.1007/s11666-024-01843-y.

[18] A. Roy, V. Jalilvand, S. Mohammadkhani, P. Patel, A. Dolatabadi, L. Roue, D. Guay, R.R. Chromik, C. Moreau, P. Stoyanov, Enhanced wear resistance of cobalt oxide over nickel oxide, Tribol. Lett. 71 (2023) 99, https://doi.org/10.1007/s11249-023-01769-6.
[19] A. Roy, R.R. Chromik, C. Moreau, P. Stoyanov, Influencing factors on the lubricity of oxide coatings, Surf. Coating. Technol. 496 (2025) 131673, https://doi.org/10.1016/j.surfcoat.2024.131673.
[20] A.R. Mayer, B.C.N.M. De Castilho, F.B. Ettouil, R.R. Chromik, C. Moreau, P. P. Stoyanov, Cobalt- and chromium-oxide-based coatings: thermally spraying a glaze layer, Tribol. Lett. 72 (2024) 129, https://doi.org/10.1007/s11249-024-01927-4.
[21] S. Goel, S. Björklund, N. Curry, U. Wiklund, S. Joshi, Axial suspension plasma spraying of Al2O3 coatings for superior tribological properties, Surf. Coating. Technol. 315 (2017) 80–87, https://doi.org/10.1016/j.surfcoat.2017.02.025.
[22] G. Darut, F. Ben-Ettouil, A. Denoirjean, G. Montavon, H. Ageorges, P. Fauchais, Dry sliding behavior of Sub-Micrometer-Sized suspension plasma sprayed ceramic oxide coatings, J Therm Spray Tech 19 (2010) 275–285, https://doi.org/10.1007/s11666-009-9415-1.
[23] W.C. Oliver, G.M. Pharr, An improved technique for determining hardness and elastic modulus using load and displacement sensing indentation experiments, J. Mater. Res. 7 (1992) 1564–1583, https://doi.org/10.1557/JMR.1992.1564.
[24] F.H. Stott, The role of oxidation in the wear of alloys, Tribol. Int. 31 (1998) 61–71, https://doi.org/10.1016/S0301-679X(98)00008-5.
[25] N.C. Ferreri, S.C. Vogel, M. Knezevic, Determining volume fractions of γ, γ′, γ″, δ, and MC-carbide phases in Inconel 718 as a function of its processing history using an advanced neutron diffraction procedure, Materials Science and Engineering: A 781 (2020) 139228, https://doi.org/10.1016/j.msea.2020.139228.
[26] A. Bansal, S. Zafar, A.K. Sharma, Influence of heat treatment on microstructure of Inconel 718 microwave clads, Surf. Eng. 33 (2017) 167–174, https://doi.org/10.1080/02670844.2016.1197559.
[27] M. Samii Zafarghandi, S.M. Abbasi, A. Momeni, Effects of Nb on hot tensile deformation behavior of cast Haynes 25 Co-Cr-W-Ni alloy, J. Alloys Compd. 774 (2019) 18–29, https://doi.org/10.1016/j.jallcom.2018.09.301.
[28] H.M. Tawancy, V.R. Ishwar, B.E. Lewis, On the fcc → hcp transformation in a cobalt-base superalloy (Haynes alloy No. 25), J. Mater. Sci. Lett. 5 (1986) 337–341, https://doi.org/10.1007/BF01748098.
[29] M. Gao, R.P. Wei, Grain BOUNDARY NIOBIUM CARBIDESIN INCONEL 718, Scr. Mater. 37 (1997), https://doi.org/10.1016/S1359-6462(97)00373-4.
[30] Y. Zhang, Z. Li, P. Nie, Y. Wu, Carbide and nitride precipitation during laser cladding of Inconel 718 alloy coatings, Opt Laser. Technol. 52 (2013) 30–36, https://doi.org/10.1016/j.optlastec.2013.03.023.
[31] C.K. Soundararajan, D. Wang, A. Vinogradov, Effect of hydrogen on nanomechanical properties of Inconel 625 studied using in-situ electrochemical nanoindentation technique, J. Alloys Compd. 948 (2023) 169742, https://doi.org/10.1016/j.jallcom.2023.169742.
[32] K. M.P.G, R.A. A, C.P. Mohanty, A.S. Chauhan, Exploring the machined surface characteristics of Haynes 25 superalloy: cost mitigation and quality enhancement perspective, Surf. Interfaces 52 (2024) 104912, https://doi.org/10.1016/j.surfin.2024.104912.
[33] K.N. Amato, S.M. Gaytan, L.E. Murr, E. Martinez, P.W. Shindo, J. Hernandez, S. Collins, F. Medina, Microstructures and mechanical behavior of Inconel 718 fabricated by selective laser melting, Acta Mater. 60 (2012) 2229–2239, https://doi.org/10.1016/j.actamat.2011.12.032.
[34] B. Rivas-Murias, V. Salgueiriño, Thermodynamic CoO-Co_3O_4 crossover using Raman spectroscopy in magnetic octahedron-shaped nanocrystals: Thermodynamic CoO-Co_3O_4 crossover using Raman spectroscopy, J. Raman Spectrosc. 48 (2017) 837–841, https://doi.org/10.1002/jrs.5129.
[35] J. Birnie, C. Craggs, D.J. Gardiner, P.R. Graves, Ex situ and in situ determination of stress distributions in chromium oxide films by Raman microscopy, Corros. Sci. 33 (1992) 1–12, https://doi.org/10.1016/0010-938X(92)90014-T.
[36] Q. Li, Y. Gou, T.-G. Wang, T. Gu, Q. Yu, L. Wang, Study on local Residual stress in a nanocrystalline Cr2O3 coating by micro-Raman spectroscopy, Coatings 9 (2019) 500, https://doi.org/10.3390/coatings9080500.
[37] B.T. Sone, X.G. Fuku, M. Maaza, Physical & electrochemical properties of Green Synthesized Bunsenite NiO nanoparticles via Extracts, Int. J. Electrochem. Sci. 11 (2016) 8204–8220, https://doi.org/10.20964/2016.10.17.
[38] S. Mo, S. Li, H. Xiao, H. He, Y. Xue, M. Zhang, Q. Ren, B. Chen, Y. Chen, D. Ye, Low-temperature CO oxidation over integrated penthorum chinense-like $MnCo_2O_4$ arrays anchored on three-dimensional Ni foam with enhanced moisture resistance, Catal. Sci. Technol. 8 (2018) 1663–1676, https://doi.org/10.1039/C7CY02474F.
[39] K.J. Kim, T.Y. Koh, Cationic structure and charge transport in sol–gel-derived nickel-cobaltite thin films, J. Sol. Gel Sci. Technol. 77 (2016) 528–533, https://doi.org/10.1007/s10971-015-3878-y.
[40] J. Deng, J. Lei, G. Wang, L. Zhong, M. Zhao, Z. Lei, Experimental investigation of cobalt deposition on 304 Stainless Steel in Borated and Lithiated high-temperature Water, Materials 16 (2023) 3834, https://doi.org/10.3390/ma16103834.
[41] B.D. Hosterman, Raman Spectroscopic Study of Solid Solution Spinel Oxides, University of Nevada, Las Vegas, https://doi.org/10.34917/2476131.n.d.
[42] K.R. Sharma, N.S. Negi, Doping effect of cobalt on various properties of nickel oxide prepared by solution Combustion method, J Supercond Nov Magn 34 (2021) 633–645, https://doi.org/10.1007/s10948-020-05753-2.
[43] Y. Li, W. Qiu, F. Qin, H. Fang, V.G. Hadjiev, D. Litvinov, J. Bao, Identification of cobalt oxides with Raman Scattering and Fourier Transform Infrared spectroscopy, J. Phys. Chem. C 120 (2016) 4511–4516, https://doi.org/10.1021/acs.jpcc.5b11185.
[44] A. Viat, G. Guillonneau, S. Fouvry, G. Kermouche, S. Sao Joao, J. Wehrs, J. Michler, J.-F. Henne, Brittle to ductile transition of tribomaterial in relation to wear response at high temperatures, Wear 392–393 (2017) 60–68, https://doi.org/10.1016/j.wear.2017.09.015.
[45] H.A.E. Hagelin-Weaver, G.B. Hoflund, D.M. Minahan, G.N. Salaita, Electron energy loss spectroscopic investigation of Co metal, CoO, and Co3O4 before and after Ar+ bombardment, Appl. Surf. Sci. 235 (2004) 420–448, https://doi.org/10.1016/j.apsusc.2004.02.062.
[46] P.J. Blau, On the nature of running-in, Tribol. Int. 38 (2005) 1007–1012, https://doi.org/10.1016/j.triboint.2005.07.020.
[47] F.H. Stott, High-temperature sliding wear of metals, Tribol. Int. 35 (2002) 489–495, https://doi.org/10.1016/S0301-679X(02)00041-5.
[48] W.J. Tomlinson, A. Easterlow, KINETICS and MICROSTRUCTURE of OXIDATION of CoO to CO304 at 700-800°C, n.d.
[49] V.G. Hadjiev, M.N. Iliev, I.V. Vergilov, The Raman spectra of Co_3O_4, J. Phys. C Solid State Phys. 21 (1988) L199–L201, https://doi.org/10.1088/0022-3719/21/7/007.
[50] S.V. Koniakhin, O.I. Utesov, A.G. Yashenkin, Raman peak shift and broadening in crystalline nanoparticles with lattice impurities, Diam. Relat. Mater. 146 (2024) 111182, https://doi.org/10.1016/j.diamond.2024.111182.
[51] Y. Qi, X. Xiao, Y. Mei, L. Xiong, L. Chen, X. Lin, Z. Lin, S. Sun, B. Han, D. Yang, Y. Qin, X. Qiu, Modulation of Brønsted and Lewis Acid centers for $Ni_xCo_{3-x}O_4$ spinel Catalysts: towards efficient Catalytic Conversion of Lignin, Adv Funct Materials 32 (2022) 2111615, https://doi.org/10.1002/adfm.202111615.